LBL-9596
CONF-790878--1

Lawrence Berkeley Laboratory
UNIVERSITY OF CALIFORNIA

Materials & Molecular
Research Division

Presented at the Conference of International Summer
Institute in Surface Science, Milwaukee, WI,
August 13-17, 1979

SURFACE AND ADSORBATE STRUCTURAL STUDIES BY PHOTOEMISSION IN THE $h\nu$ = 50-500 eV RANGE

David A. Shirley

August 1979

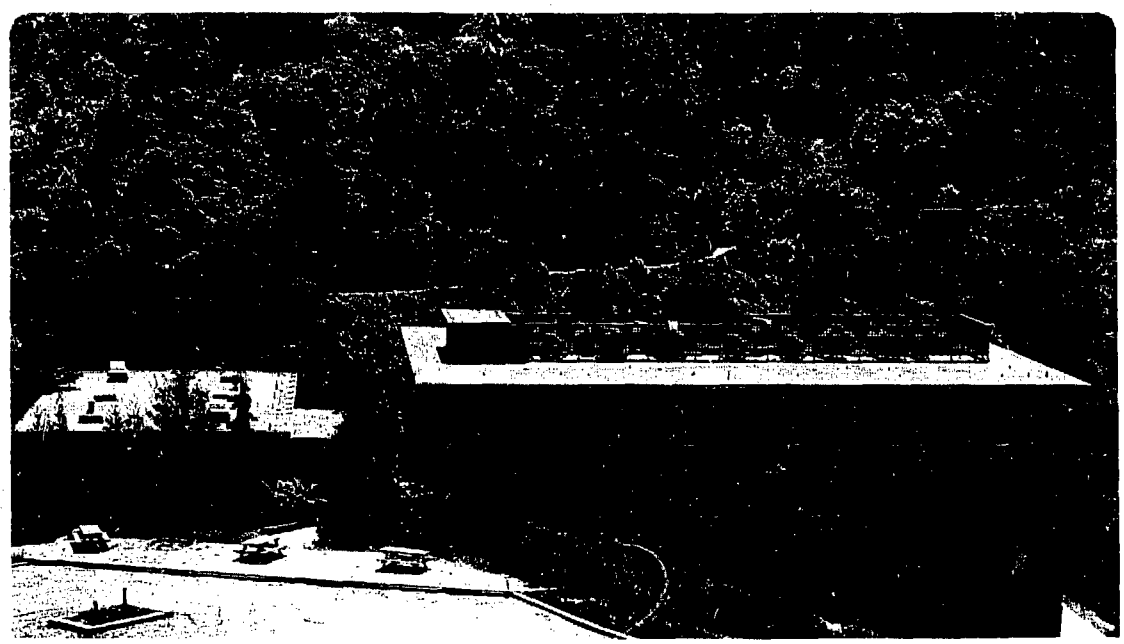

Prepared for the U. S. Department of Energy
under Contract W-7405-ENG-48

SURFACE AND ADSORBATE STRUCTURAL STUDIES BY PHOTOEMISSION IN THE hν = 50-500 eV RANGE

David A. Shirley

Materials and Molecular Research Division
Lawrence Berkeley Laboratory
and
Department of Chemistry
University of California
Berkeley, California 94720

August 1979

Abstract: The present status of photoelectron spectroscopy in the 50-500 eV range is discussed in relation to its application to surface science. Instrumentation aspects of synchrotron radiation sources are reviewed. The direct transition model is shown to be applicable in this range with some limitations. Cooper minima and adsorbate sensitivity enhancement for hν > 100 eV are reviewed. A new effect--condensed phase photoelectron asymmetry--is noted. Finally, photoelectron diffraction--another new effect--is described and evaluated.

Outline

I. Introduction

II. Photoemission in the 50-500 eV Range

A. Experimental Aspects of Synchrotron Radiation Sources

B. Photoemission From Clean Surfaces: Selected Results

III. Atomic Photoemission Behavior in Solids

A. Adsorbate Sensititivy Enhancement

B. Condensed-Phase Photoelectron Asymmetry

IV. Photoelectron Diffraction

A. Azimuthal Photoelectron Diffraction

B. Normal Photoelectron Diffraction

I. INTRODUCTION

The advent of intense synchrotron radiation sources covering any new region of the electromagnetic spectrum provides opportunities that surface scientists should explore. This is especially true for the photon energy region 50-500 eV, which is addressed in this paper. For several reasons, this region shows special promise.

Progress in experimental surface science during the last decade can be attributed to two factors: dissemination of the ability to produce and characterize clean surfaces, and development of sensitive techniques for studying these surfaces. A major component of the latter is the field which can be generically termed electron spectroscopy, in which outgoing electrons are detected following energy (and often momentum) analysis. Electron spectroscopy techniques are usually categorized by more-or-less descriptive acronyms such as UPS, XPS, ESCA, LEED, AES, etc. A number of quite pointless discussions have been devoted to comparing the relative surface sensitivities of these techniques. A more meaningful assessment can be made by comparing the techniques at equivalent kinetic energies of the outgoing electrons. In this context it is clear that the surface sensitivities of these electron spectroscopies are derived from their short mean free paths of less than 10 Å in the kinetic energy range ∿20-200 eV. Any given technique tends to be surface

sensitive to the extent that it involves detection of electrons in this energy range. Thus, AES may be more surface-sensitive for one material and XPS for another.

Specializing now to photoemission, the standard laboratory photon sources tend to eject electrons with energies that are either too low ($\sim$10 eV in the case of UPS) or too high ($\sim$1000 eV in XPS) to give the best surface sensitivity. While this point can be successfully challenged for many specific cases, it nonetheless is usually true that for optimal surface sensitivity one would prefer to have the facility of tuning the electron kinetic energy K within or through the surface sensitive energy region $\sim$20-200 eV. From the Einstein relation

$$K = h\nu - E_B$$

this is readily achieved for any given orbital binding energy E_B if the photon energy $h\nu$ is tunable. Because valence bands and adsorbate molecular orbitals have E_B values typically in the range 0-30 eV, and most elements have core levels with E_B of a few hundred eV or less, it follows that tunable synchrotron radiation sources in the 50-500 eV range are of unique interest in connection with surface science studies by photoemission.

In 1974 radiation in this energy range became available at the Stanford Synchrotron Radiation Laboratory (SSRL),[1] based on the SPEAR storage ring. It was monochromatized

by a grazing-incidence "grasshopper" monochromator due to F.C. Brown et al.[2] as part of the 4° branch of Beam Line I, which was implemented by the Xerox Palo Alto Research Center. Since 1974, in spite of the severe handicap of parasitic operation, several groups have carried out pioneering[3] experiments in surface science on this facility. More recently, the groups of Y. Petroff et al. at LURE and of N. Smith et al. at Tantalus have done surface science photoemission studies in the energy region around 100 eV. From this growing body of work we have selected for discussion below a subset of studies defined by the conditions that they involve photoemission, and that they specifically require synchrotron radiation in the 50-500 eV range. Even with these restrictions, choices were necessary. We have, for example, omitted semiconductor interface studies, which were reviewed recently by Lindau and Spicer.[4]

The discussion below is presented in three sections. General comments about photoemission in the 50-500 eV range appear in Section II, supported by specific observations drawn from SSRL. The atomic nature of certain photoemission phenomena in this range is noted and discussed in Section III. Finally, photoelectron diffraction--a new effect--is treated in Section IV.

II. PHOTOEMISSION IN THE 50-500 eV RANGE

This topic will be treated in two parts. Section II.A. describes experimental parameters on the SSRL 4° branch line in a summary manner, and Section II.B. cites the results of recent studies on clean surfaces at SSRL, Tantalus, and LURE that are of special interest in delineating the applicability of the technique.

A. Experimental Aspects of Synchrotron Radiation Sources

The important parameters that characterize photon sources for photoemission are intensity, resolution, spot size, polarization, time structure, spectral purity, and various factors related to steadiness and reliability of the beam. These parameters are of little direct interest to the surface scientist, but they become critical, and usually limiting, when planning and executing photoemission experiments in the 50-500 eV range. We shall describe briefly the present status of these parameters for the 4° branch at SSRL, which is the only beam line in the world with a long history of photoemission in this range. New lines are planned or underway in several laboratories, and some of these parameters should be improved in most of them, as well as at SSRL, in the near future. Nevertheless, the present comments can serve as a useful baseline.

Observations about this branch line are widely scattered in the literature, but surface scientists would find a

considerable amount of useful information in three sources: Ref. 2, describing the line, a report on "beam line chemistry" by the present author,[5] and a report by Stöhr and Johansson[6] on the performance of the grasshopper monochromator in the 280-1000 eV range.

Stöhr and Johansson have given the absolute flux of the line as ranging between 1 and 10 in units of 10^8 photons sec^{-1} ΔE^{-1}, where $\Delta E = C \times 10^{-6} E^2$, as given by Brown et al.,[2] is the band pass of the grating (C = 16 for 600 lines/mm; C = 8 for 1200 lines/mm). These figures were quoted for newly installed optical elements and for colliding-beam operation at 1.84 GeV and 10 mA at SPEAR. Dedicated operation should improve these intensities by about a factor of 100, and similar fluxes should soon be available at other facilities. Stöhr and Johansson gave the energy dependence of the photon flux for several sets of conditions. In Fig. 1 we show a typical curve illustrating the photon flux as measured by the photocurrent on a calibrated NBS photodiode for the 4° branch line with "old" optical surfaces.

We may summarize the photon intensity situation as follows. Combining the above figure with typical photoelectric cross-sections in the 50-500 eV region, and taking due account of various detector sensitivity factors, one concludes that the presently available fluxes of 10^8 - 10^9 sec^{-1} are barely acceptable for surface-science studies. Indeed, experiment has borne this out; thus far it has usually been necessary

to concentrate on a few carefully chosen prototype systems. An intensity increase by a factor of 100 or more will improve this situation dramatically.

The spectral purity factor comes up in an insidious way. Referring to Fig. 1, one must remember that a photodiode is a nondispersive detector. Thus, at any energy there are contributions present from second- and higher-order light as well as from scattered light. Photoelectron spectroscopy is dispersive, of course, by virtue of electron energy analysis; but extraneous light is still very troublesome. Near the optimum energy corresponding to the grating's blaze angle (150 eV in this case), spectral intensity and purity are good. At lower energies, higher-order reflections present serious problems. Above 280 eV, however, extremely severe difficulties are encountered, and we are immediately thrust into the realm of surface chemistry.

The carbon K-edge lies near 280 eV.[7] No carbon is present in clean optical elements, but carbonaceous deposits build up as beam lines are used, and their performance deteriorates. This will be a major obstacle to surface studies above $h\nu$ = 280 eV, an important region in which the carbon, nitrogen, and oxygen K-edges lie. The gravity of the problem is evident on careful inspection of Fig. 1. A big dip in the photon flux at 280 eV is apparent in the curve, for "old" optical elements. Furthermore, there is essentially no recovery above 280 eV. In fact the remaining intensity at

higher energies is largely due to higher-order and scattered light. The carbon buildup that this curve implies occurs in an ultrahigh vacuum beam line at pressures in the 10^{-9} Torr range. New optical elements show a smaller dip and better recovery, but the performance depicted in Fig. 1 is reached within a few weeks. To explain it, we start with the seemingly outrageous statement that this beam line contains all the essential ingredients of a low-grade catalytic converter!

The reasoning behind this statement is simple. There are two generic reactions which we believe to occur most frequently in beam lines. Both are well-known and widely used industrial synthesis reactions that have been studied sufficiently to allow us to draw conclusions about their occurrence and control.

First, consider Fischer-Tropsch synthesis. The desired reaction involves catalytic combination of CO and H_2 to form hydrocarbons. An unwanted side reaction is

$$2\ CO \rightarrow CO_2 + C,$$

with a gaseous and a solid product. This is a catalytic reaction, but it does not proceed at ambient temperatures even in the presence of a platinum or nickel catalyst. Why, then, is it a problem in ambient-temperature beam lines?

To provide an answer, we note that the material ingredients for Fischer-Tropsch synthesis are all present. Both CO and H_2 are ubiquitous constituents of ultrahigh vacuum

systems. In fact, they remain behind after all other gases have been eliminated. Mirror surfaces are usually coated with transition metals (e.g., Os, Pt) which serve as catalysts. Finally, UV or soft x-ray irradiation replaces thermal excitation in initiating bond cleavage. Evidence that the radiation is necessary is provided by the fact that carbonaceous discoloration of optical elements occurs only on the regions where the beam strikes.

The reaction given above yields activated carbon, tenaciously bound to the substrate. Its subsequent fate in a Fischer-Tropsch reactor depends on ambient conditions. It can serve as the starting point for hydrocarbon synthesis, in the presence of suitable reactants. However, in an ultrahigh vacuum system, in the presence of additional radiation (or at high temperatures), it reacts to form graphitic overlayers. Unfortunately, these overlayers build up even on gold.[8] Thus replacement of catalytic transition metals by gold will not completely solve the problem, though some improvement should be realized.

In addition to Fischer-Tropsch synthesis, catalytic cracking of hydrocarbons may take place in ultrahigh vacuum lines, with the hydrocarbons being produced by the Fischer-Tropsch process. Again, activated carbon is formed via processes such as

$$C_3H_8 \xrightarrow{h\nu,\ Pt} 2\ CH_4 + C$$

$$\longrightarrow CH_4 + 2\ H_2 + 2\ C$$

etc. Subsequent formation of graphite would proceed as before. Baker and co-workers have used electron microscopy to observe very long filaments of carbonaceous material formed on nickel particles during the cracking of propane.[9]

We deduced that the dip at 280 eV in Fig. 1 could be attributed to absorption by graphite by comparing an expanded and inverted plot of the transmission function to a polycrystalline graphite absorption spectrum,[5-7] as shown in Fig. 2. The similarity of these two curves is striking. We concluded that the overlayers on optical elements in the beam line are at least in large part graphitic rather than, for example, carbidic or polymeric. It seems clear that similar overlayers will be encountered in other beam lines, so this may be a general problem above 280 eV. Furthermore, the derived mean total overlayer thickness[7] of 25 Å implies loss of intensity even in lower-energy beam lines at vacuum ultraviolet energies.

Our additional comments about the photon source will be brief. Resolution is generally traded off against intensity in optical systems. Spot size at the focal "point" is also important in photoemission experiments, both because most electron analyzers accept and analyze electrons only from small areas and because angular resolution is only meaningful if the effective electron source size is no larger than the analyzer entrance slit. A fixed focal point for the radiation after leaving the monochromator is therefore mandatory. In

practice spot sized of 0.1-1 mm diameter can usually be achieved while meeting this condition.

Polarization is always expected, but seldom confirmed, for synchrotron radiation in the 50-500 eV region. From anisotropic angular distributions of photoelectrons, discussed in Section III, we estimate that the radiation on the 4° branch line at SSRL is at least 98% polarized at $h\nu$ = 200 eV. This can have exciting consequences for surface-science application.

The photon beam intensity fluctuates with time. Only a portion of the synchrotron radiation is transmitted through each successive optical element, and the spectral composition of the beam varies with transverse distance. Thus, small instabilities in the circulating storage-ring current can be amplified in unpredictable ways before the photon beam reaches the photoelectron spectrometer. For accurate measurements a photon beam monitor is essential. We have found that intensity fluctuations at $\sim$1 Hertz are never less than ±1%. The (photon)/(ring current) ratio can deviate by much larger amounts over longer periods.

Finally, we address the time structure of the source in the context of considering the electron analyzer, a closely related problem. It is important to note that photoemission from surfaces is manifestly a three-vector problem at its simplest, and more generally a five-vector problem. The radiation vector potential $\vec{A}$ must always be considered,

as must the photoelectron's momentum vector $\vec{p}$ and the surface normal $\vec{n}$. To these we must add vectors to describe crystallographic axes and/or adsorbate orientation. Clearly, it is desirable to control the relative orientation of these vectors by moving the analyzer and sample. In our research group this has been achieved by a hemispherical analyzer with two-circle rotation which is "semidispersive" in that it analyzes and collects electrons over a small energy range by means of a two-dimensional resistive strip.[10]

The time-structure of SPEAR also provides an alternative approach: electron energy analysis by time-of-flight (TOF) techniques. An early TOF analyzer was developed by the Xerox group,[11] and used to prove the feasibility of this approach at SSRL. Recently high-resolution, high-efficiency performance has been obtained on another beam line in TOF studies on gases.[12] It appears that the TOF approach offers the possibility of enhancing the detection efficiency of photoelectron analyzers by a factor of 10^2 - 10^3 over ordinary single-channel analysis--a very worthwhile improvement. While the pulse structure of SPEAR (300 psec pulse width at 780 nsec intervals) is particularly well-suited to TOF detection, other present and planned storage rings have timing characteristics that should allow this approach as well.

B. Photoemission From Clean Surfaces: Selected Results

In this subsection we review briefly the main salient features of photoemission from clean surfaces that have been established in the 50-500 eV range to date. A more extensive review of the earlier aspects has appeared elsewhere,[13] and they will be discussed only briefly below.

First, we state the obvious fact that bulk spectroscopic properties of any sample must be understood if one is to study its surface spectroscopy. This follows because a major portion of the spectral intensity often comes from the bulk, even for surface-sensitive techniques.

Most early photoemission experiments were carried out in an angle-integrated mode or on polycrystalline samples, yielding angle-averaged spectra. For some types of study--e.g., dispersed particulates--this will continue to be the case. Thus, one of the first questions addressed by photoemission in the 50-500 eV range was the energy boundary between the UPS and the XPS regions. The former is characterized by the spectra appearing as a joint (initial and final) density of states (JDOS), while the latter was expected to set in when the final states became so dense as to effect a complete sampling of the valence band, yielding a spectrum resembling the valence-band density of states (VBDOS). In fact, photoemission studies of copper for the range $h\nu$ = 40-200 eV[14] have shown that the XPS-DOS limit is reached

for this case at $h\nu \sim 100$ eV. Except for cases in which modulation by atomic effects is important,[15,16] similar behavior can be expected for other materials.

Angle-resolved photoemission is a different matter. The first systematic angle-resolved studies of single crystals in this energy range were carried out at SSRL on Cu and Au.[17] They showed very marked variations of spectral shape with photon energy, as well as large differences with direction of electron propagation relative to the crystalline axes. These observations were ultimately understood in terms of the direct-transition model (DTM).[13,18,19] At first it was rather surprising that the DTM would be applicable at these high photon energies, but it now appears that the DTM fit will apply to many materials. As an example of the detail in which angle-resolved photoemission spectra can be fitted to the DTM, we show in Fig. 1 a plot of the copper valence bands along the Λ line,[20] fitted over the photon energy range $h\nu$ = 7-200 eV. The agreement is remarkable. The exact scope and limit of the DTM in the $h\nu$ = 50-500 eV range is one of the most important questions remaining in photoemission.

One unavoidable limit on the DTM fit is thermal diffuse scattering (TDS), by means of which phonon momentum couples to the photoelectron system, breaking the selection rule that equates initial- and final-state k vectors. The dramatic way in which TDS can affect an angle-resolved photoemission spectrum is illustrated in Fig. 4. Here the normal Cu(110)

valence-band spectrum is shown as a function of temperature, for $h\nu = 45$ eV.[21] The sharp features observed at room temperature are due to sampling of a very limited region in the Brillouin zone. Heating the sample leads to sampling of much more of the zone, and the spectrum goes over into density-of-states type appearance. The reason for this is that the ratio of indirect to direct transition intensity is controlled by the Debye-Waller factor,

$$f = \exp[-\langle (\vec{q}\cdot\Delta\vec{r})^2 \rangle]$$

Here $\vec{q}$ is the momentum of the photoelectron and $\Delta\vec{r}$ is the instantaneous thermal displacement of an atom in the lattice. The functional dependence of f upon $\vec{q}$ and $\Delta\vec{r}$ tells us that these two parameters are equivalent. Thus, to maximize the DTM mechanism we should work at low photon energies and/or temperatures. In fact for most materials the lattice stiffness is such that photon energies up to $h\nu \sim 100$ eV are acceptable at room temperature, and $h\nu \sim 500$ eV may be tolerated for some, but the true laboratory-source XPS regime, $h\nu > 1000$ eV, will practically eliminate direct transitions. Similar effects are well-known in x-ray crystallography, and of course in LEED studies. Cooling the sample helps, but zero-point motion sets a lower limit on $\langle \Delta r^2 \rangle$ and limits the improvement that can be realized. Although these arguments pertain to bulk solids, similar considerations apply to adsorbate systems.

The applicability of the DTM analysis to semiconductors has received a lot of attention lately. Grandke et al.[22] have put forth a model in which a one-dimensional density of states (ODDOS) picture was used to explain photoemission spectra of PbS at a photon energy of $h\nu = 21.2$ eV. The idea was that $k_\perp$ was not a good quantum number because of the shallow sampling depth at this energy. In a later report these authors employed a unified DTM/ODDOS model[23] for the lead salts. Thiry et al.[24] studied PbSe at various photon energies, finding that ODDOS behavior apparently sets in before $h\nu = 35$ eV as the photon energy is raised and that ODDOS spectra can be used to map bands, or at least critical points. K. Mills et al. in our laboratory have found that the DTM works well up to $h\nu \sim 20$ eV in GaAs,[25] but that for $h\nu > 20$ eV the spectra were better fitted either by a ODDOS model or possibly by a DTM analysis with very complicated final states. In fact, Eastman and co-workers have more recently carried these measurements up to $h\nu = 100$ eV, and found[26] that the simple DTM analysis works again at higher energies. One possible interpretation of all of this evidence is that the ODDOS mechanism is applicable near the minimum-escape-depth energy (typically $\sim$20-50 eV), with the DTM being operative at higher and lower energies. Clearly, more work is necessary before general statements can be made.

We touch very briefly on the subject of stepped surfaces, mainly to note we do not yet understand them. Both Cu(211)

and Pt(211) have been studied extensively in our laboratory by angle-resolved photoemission. At this writing Pt(211) shows spectra different from expectations based on a DTM analysis of the bulk bands, while Cu(211) does not. Little more can be said as yet.

This section will conclude with comments about two recent observations that have been made about surface electronic structure. Citrin et al.[27] reported a lower binding energy for Au4f electrons in the surface compared to the bulk, based on high-resolution XPS spectra and careful analysis. They also derived a surface-layer density of states for the valence band. Very recently Tran Minh Duc et al.[28] have experimentally resolved surface and bulk peaks for 4f electrons on the (110) face of tungsten. This amazing ability to resolve surface and bulk substrate features opens up many possibilities for surface-science studies.

The other remarkable observation was made by Y. Petroff et al.[29] These workers studied Cu(111) at very high energy- and angular-resolution, and found that the well-known Cu(111) surface state near the Fermi energy, which has previously been seen only at low photon energies, $h \leq 40$ eV, in fact recurs at higher energies, along with two other strong surface states. Thus, it may be possible after all to study surface states at higher energies, where surface sensitivity is greatest.

III. ATOMIC PHOTOEMISSION BEHAVIOR IN SOLIDS

A fascinating aspect of surface-science photoemission is that both itinerant and localized aspects of the electronic structure of surfaces are apparent. Both were evident in Section II.B, for example. In this section we address two aspects of atomic behavior in solids, and show how they are related to surface studies. The first is the Cooper minimum in valence-band cross-sections, which allows us to tune the sensitivity of photoemission to molecular orbitals in adsorbates, and the second is the newly discovered phenomenon of condensed-phase photoelectron asymmetry.

A. Adsorbate Sensitivity Enhancement

Bordass and Linnett[30] showed the feasibility of studying adsorbates on surfaces by ultraviolet photoelectron spectroscopy, by observing molecular orbital peaks of methanol adsorbed on tungsten. Since then many experiments have been performed and a great deal has been learned about adsorbate systems. An important factor in this work has always been the relative spectral intensity of adsorbate orbitals relative to the substrate valence band and associated inelastically scattered electrons. Synchrotron radiation provided the means of going to higher energies, where surface sensitivity might be greater, but in early studies the relative molecular orbital to valence-band intensity ratio, MO/VB, appeared to decrease catastrophically with increasing

photon energy in the limited energy range then available.[31] What was needed was a method of turning off photoemission from the valence bands of suitable substrates. In fact, such a method exists in the form of Cooper minima in photoemission cross-sections,[32,33] a phenomenon that is well-known in atomic photoemission, but unfamiliar in surface science.

The physics underlying Cooper minima is straightforward. Electric dipole selection rules ($\Delta\ell = \pm 1$) allow transitions only to p or f continuum final states from d valence bands of transition metals. Well above threshold the d → f channel is dominant, and it suffices to consider it alone. For initial-state wave functions $n\ell$ having radial nodes, the photoemission matrix element

$$\langle n\ell|\vec{A}\cdot\vec{p}|\ \varepsilon,\ell+1\rangle$$

can vanish for energies where the negative and positive contributions just cancel. This yields a minimum in $\sigma(h\nu)$--not zero, because the $\ell \rightarrow \ell-1$ channel is nonzero. Returning to the d → f case, such a minimum may occur for 4d and 5d metals, but not 3d, because of the absence of radial nodes. By tuning the photon energy to this minimum, valence-band photoemission can be effectively suppressed, and the MO/VB ratio correspondingly enhanced. Apai et al.[34] first demonstrated this effect for the system CO/Pt, and Miller et al.[35] later applied it to stepped Pt crystals. Fig. 5 shows the measured valence-band photoelectron intensities of five metals. Clearly the decrease in intensity of the 5d metals at high photon energies,

$h\nu > 150$ eV, is well-suited to enhancement of MO/VB.

An even more dramatic case is provided by the 4d series. Here the maximum in $\sigma(h\nu)$ falls at a higher energy because of the smaller radial extent of the 4d functions, but the subsequent decrease is also sharper and the minimum quite narrow. It was predicted[13] and subsequently confirmed[36] experimentally that the ratio MO/VB for the system CO/Pd should show a sharp maximum near $h\nu = 130$ eV. Figure 6 shows the variation of the photoemission spectrum with photon energy for this system. The improvement in adsorbate sensitivity is truly dramatic from $h\nu = 80$ eV to $h\nu = 130$ eV, where the CO molecular orbitals actually dominate the spectrum!

Little application has been made as yet of this approach, but more can be expected as photon sources in the $h\nu > 100$ eV range become more widely available. It should also be noted that discrete laboratory sources may also be applicable. For example, the YM_ζ line lies at $h\nu = 132$ eV.

B. Condensed-Phase Photoelectron Asymmetry

Even a review article should contain some new material. In this subsection we describe a recently discovered effect[37] that has implications for all photoelectron spectroscopy in condensed phases--namely, the dependence of the differential photoelectron cross-section, $d\sigma/d\Omega$, upon the angle α between the vector potential of the photon field, $\vec{A}$, and the photoelectron momentum, $\vec{p}$.

According to Yang's theorem,[38] the general form of the photoelectron angular distribution from a randomly oriented system excited by a vector potential $\vec{A}$, via a dipole process, is

$$\frac{d\sigma(\varepsilon)}{d\Omega} = \left[\frac{\sigma(\varepsilon)}{4\pi}\right] \left[1 + \beta(\varepsilon)P_2(\cos\alpha)\right] .$$

Here, σ is the angle-averaged cross-section, ε the photoelectron kinetic energy, and P_2 the second LeGendre Polynomial $P_2(x) = 3x^2/2 - 1/2$. The asymmetry parameter, $\beta(\varepsilon)$, has the limits $-1 \leq \beta(\varepsilon) \leq 2$, as required to insure that $d\sigma/d\Omega$ is nonnegative. In the past, Yang's theorem was applied to atoms and molecules, for which many $\beta(\varepsilon)$ values have been calculated. In condensed phases, however, photoelectron asymmetry from the source was either ignored or unknown. In ordered solids, for example, there are other important angular distribution effects. Angle-resolved photoemission from valence bands, discussed in Section II, arises via $\vec{k}$ conservation. Diffraction effects, discussed in Section IV, also arise from lattice periodicity. The $\beta(\varepsilon)$ term for a randomly oriented system has, however, received little attention.

At low photon energies (and low ε values), asymmetry effects are not usually very striking. The $\beta(\varepsilon)$ parameter is seldom near either of its limits. Asymmetry effects are smaller with laboratory sources because they are unpolarized, and even with (polarized) synchrotron radiation, the angle α

between $\vec{A}$ and $\vec{p}$ is typically fixed at some value far from 0°, so that dramatic effects that could arise through the perturbation term

$$\mathcal{H}' = \frac{e^2}{2mc^2} (\vec{A}\cdot\vec{p} + \vec{p}\cdot\vec{A})$$

are minimal. Thus the $\beta(\varepsilon)$ effects, which are very large, have gone unnoticed, or at least unremarked.

In early experiments designed to study photoemission from surfaces in s polarization, we found a great decrease in intensity. With our new movable analyzer we have been able to control the angle α and measure $\beta(\varepsilon)$ for core levels of disordered or polycrystalline materials (thereby satisfying Yang's criterion).[37] Very large effects were observed. For example, the photoelectron intensity for the Ag(4s) level increased by a factor of 25 as α was reduced from 90° to 48°. The $P_2(\cos\alpha)$ dependence was confirmed, permitting the derivation of β values. Figure 7 shows $\beta(\varepsilon)$ and $\sigma(\varepsilon)$ for the Ag(4s) and Ag(4d) shells, as well as theoretical values of these parameters calculated for xenon by Kennedy and Manson.[39] The agreement is remarkable. The 4s peak shows near maximum asymmetry--i.e., $\beta = 2$, or a $\cos^2\alpha$ distribution--while the 4d shows distinctive atomic character. At the same time, the condensed phase appears to increase the observed value of $\beta(\varepsilon)$ throughout relative to atomic expectations.

The implications of this discovery for photoemission, and surface studies in particular, are quite broad. All comparisons of elemental abundance by ESCA will have to be reevaluated, to assess the experimental α settings. Of more interest are the possibilities for controlling α to identify orbital symmetry (e.g., $\beta = 2$ for an s level) or to enhance certain peaks (e.g., adsorbate MO's). The applications are many and obvious and need not be elaborated here.

IV. PHOTOELECTRON DIFFRACTION

A second major reason for interest in photoemission in the $h\nu = 50$-500 eV region on the part of surface scientists, in addition to surface sensitivity, is the fact that photoelectrons in the 100 eV energy range have de Broglie wavelengths comparable to atomic dimensions. Thus photoelectron diffraction[40] is possible for adsorbate-substrate systems; the physics of this diffraction is similar to LEED, but selection of a given photoelectron peak would make the experiment more specific to the geometry of a particular element.

The first experimental proof of photoelectron diffraction was obtained on molecular orbital peaks of CO on Pt(111), in normal emission.[13] This result was not susceptible to straightforward analysis, however. More recently a number of adsorbate systems have been found to exhibit photoelectron diffraction. It is convenient to divide the subject into two parts at this point. Azimuthal photoelectron diffraction

(APD) will be treated in Section A, and normal photoelectron diffraction (NPD) in Section B.

A. Azimuthal Photoelectron Diffraction

In this experiment photoelectrons from a given adsorbate level are collected at a given fixed photon energy, and (nonzero) polar angle θ. The azimuthal angle, ϕ, is varied either through the entire range $0 \leq \phi \leq 2\pi$ or through some suitable fraction $2\pi/n$, where n is the repeat period of the system, dictated by symmetry (e.g., n = 4 for C_4 symmetry or for C_{2v}, etc.). In practice, it is preferable to vary ϕ through the entire range $0 - 2\pi$, for experimental reasons.

Two groups have carried out APD studies to date. Woodruff, Smith, and co-workers[41] used synchrotron radiation in the range $h\nu$ = 80-100 eV to study c(2×2)Te/Ni(001) and c(2×2)Na/Ni(001), with $\theta = 30°$ typically. Intensity modulations of up to 50% were observed on the Te4d and Na2p peaks as ϕ was varied. The "flower patterns" of $\sigma(\phi)$ as obtained showed the overall point-group symmetry of the system in each case. At these relatively low photon energies, multiple scattering effects are important, and interpretation requires a full-scale analysis by dynamical LEED theory. The sensitivity of the low-energy APD spectra to relative adsorbate-substrate geometry is unclear as yet. It is also not proved that structural determinations by this method will be feasible. At this writing the method has been extended to several

systems--e.g., Se on Ni(111)[42]--and it is being pursued both experimentally and theoretically.

High-energy APD has been carried out by C.S. Fadley et al.,[43,44] who used a laboratory x-ray source ($h\nu$ = 1487 eV). These workers studied the system c(2×2)O/Cu(001), and found effects up to 41% as ϕ was varied. They used a simplified single-scattering model to analyze their data, which were obtained at several fixed values of θ. It was argued that multiple scattering effects are negligible at these high energies. A structure was derived for O/Cu(001) in which oxygen atoms were deduced to lie in fourfold coordination sites coplanar with the surface layer of copper atoms. At this writing the generality of this method is not clear, but it has yielded a structure, and it has the advantages of a simple theory and of requiring only a laboratory source.

B. Normal Photoelectron Diffraction

This is the technique by which photoelectron diffraction was first observed,[13] and its particular merits have been emphasized by S.Y. Tong and co-workers.[45-48] It requires a variable-energy photon source, and a theoretical analysis of intermediate complexity.[49] The angles θ and ϕ of the photoelectrons that are analyzed are held fixed at $\theta = 0°$. The effects that are directly observed are very large: The normal photoelectron intensity has been observed to vary by as much as a factor of three with increasing photon energy.

This is a consequence of the fact that the NPD intensity is a coherent superposition of several LEED beams, measured in the direction of highest symmetry. Figure 8 shows the magnitude of the NPD effect in a series of raw spectra for the system p(2×2)Se/Ni(001). Two features are notable in this figure: the remarkable surface sensitivity, which allows a quarter-monolayer selenium coverage to yield a major peak, and the large modulation of peak intensities. The latter is displayed in Fig. 9 for the Ni substrate valence-band and 3p peaks, as well as for the Se(3d) peak, as given by S.D. Kevan et al.[50]

The NPD spectra show excellent agreement with theory for the systems p(2×2)Se/Ni(001) and c(2×2)Se/Ni(001), the systems that have been analyzed in detail.[48,51] A number of other systems have been studied[52,53] and have yielded promising curves, suggesting that they, too, will provide unambiguous structures. They are listed in Table I. For both of the systems given above, the data yielded d_1, the adsorbate-surface interplanar distance, directly, and established the Se atoms as lying in fourfold hollow sites. A strong feature of NPD is that d_1 follows from the positions of the intensity maxima, rather than from their amplitudes.

Although NPD is a new technique, it is already quite promising as a structural method. It seems to be applicable to a wide range of systems, as shown in Table I. It can yield structures, and it is applicable to disordered or very

low-coverage overlayer systems (which LEED is not). Figure 10 compares low-coverage and ordered Se/Ni(001) NPD curves, showing that the effect is retained for disordered overlayers. Further work is required to evaluate NPD, APD, and the other phenomena discussed in this paper, but it appears probable that photoemission in the $h\nu$ = 50-500 eV range with be of considerable interest to surface science.

ACKNOWLEDGMENTS. It is a pleasure to acknowledge the members of my research group, past and present, who have made the exploration of the $h\nu$ = 50-500 eV range an exciting adventure. Their contributions are duly recognized in the references to original publications, but I wish to acknowledge particularly R.F. Davis for the $\beta(\varepsilon)$ work, S.D. Kevan for the NPD studies, and D.H. Rosenblatt for assistance with the illustrations.

This work was supported by the Division of Chemical Sciences, Office of Basic Energy Sciences, U.S. Department of Energy under Contract No. W-7405-Eng-48. It was performed at the Stanford Synchrotron Radiation Laboratory, which is supported by the NSF Grant No. DMR 77-27489, in cooperation with the STanford Linear Accelerator Center.

Table I

Systems Studied by NPD

System	Level	Reference
p(2×2)Se/Ni(001)	Se(3d)	51
c(2×2)Se/Ni(001)	Se(3d)	51
Se/Ni(001)-low coverage	Se(3d)	50
c(2×2)S/Ni(001)	S(2p)	50
c(2×2)Se/Ni(110)	Se(3d)	52
c(2×2)S/Ni(110)	S(2p)	52
Se/Ni(111)-low coverage	Se(3d)	52
$\sqrt{3} \times \sqrt{3}$ Se/Ni(111)	Se(3d)	52
CO/Ni(001)	C(1s)	52
CO/Ni(111)	C(1s)	52
c(2×2)Na/Ni(001)	Na(2p)	53

REFERENCES AND NOTES

(1) Until 1978 the name was Stanford Synchrotron Radiation Project.

(2) F.C. Brown, R.Z. Bachrach, S.B.M. Hagström, N. Lien, and C.H. Pruett in "Vacuum Ultraviolet Radiation Physics," E.E. Koch, R. Haensel, and C. Kunz, Eds., Pergamon, Vieweg, 1974, p 785; F.C. Brown, R.Z. Bachrach, and N. Lien, Nucl. Instrum. Methods 152, 73 (1978).

(3) Among the major users in the surface science area are the Xerox PARC group (S.B.M. Hagström, R.Z. Bachrach, R. Bauer et al.); three Stanford/SSRL groups led by W.E. Spicer, by I. Lindau, and by J. Stöhr; the China Lake group (V. Rehn); and our own. The term "pioneering" is used not only in the positive sense of acknowledging that many new types of experiment have been done, but also to indicate that higher fluxes and better operating conditions in future dedicated operations will permit more extensive, higher-resolution studies in the near future.

(4) I. Lindau and W.E. Spicer, J. Electr. Spect. and Rel. Phenomena 15, 295 (1979).

(5) D.A. Shirley, "Beam Line Chemistry," Lawrence Berkeley Laboratory Report LBL-7636 (1978); also in Proceedings of the International Workshop on X-Ray Instrumentation, SSRL Report No. 78/04, Stanford University, 1978 (unpublished), pp VII-80.

(6) J. Stöhr and L.I. Johansson, "Performance of the Grasshopper Monochromator in the Soft X-Ray Region 280-1000 eV." (Nuclear Instruments and Methods, to be published 1979)

(7) D. Denley, P. Perfetti, R.S. Williams, D.A. Shirley, and J. Stöhr, "Carbon K-Edge Fine Structure in Graphite Foils and in Thin-Film Contaminants on Metal Surfaces," Lawrence Berkeley Laboratory Report LBL-9431, July 1979. (Submitted to Phys. Rev. B)

(8) A.E. Morgan and G.A. Somorjai, Surface Science 12, 405 (1968).

(9) C.W. Keep, R.T.K. Baker, and J.A. France, J. Catalysis 47, 2326 (1977), and references cited therein.

(10) This spectrometer was developed in collaboration with F.R. McFeely of MIT. Our machine was built by S.D. Kevan. D. Malone of LBL did the mechanical design and J.E. Katz did the electronics design.

(11) R.Z. Bachrach, F.C. Brown, and S.B.M. Hagström, J. Vac. Sci. Tech. 12, 309 (1975).

(12) M.G. White, R.A. Rosenberg, G. Gabor, E.D. Poliakoff, G. Thornton, S.N. Southworth, and D.A. Shirley, "Time-of-Flight Photoelectron Spectroscopy of Gases Using Synchrotron Radiation," Lawrence Berkeley Laboratory Report LBL-8851, March 1979. (Review of Scientific Instruments, to be published)

(13) D.A. Shirley, J. Stöhr, P.S. Wehner, R.S. Williams, and G. Apai, Physica Scripta 16, 398 (1977).

(14) J. Stöhr, F.R. McFeely, G. Apai, P.S. Wehner, and D.A. Shirley, Phys. Rev. B14, 4431 (1976).

(15) I. Lindau, P. Pianetta, K.Y. Yu, and W.E. Spicer, Phys. Rev. B13, 492 (1976).

(16) P.S. Wehner, J. Stöhr, G. Apai, F.R. McFeely, R.S. Williams, and D.A. Shirley, Phys. Rev. B14, 2411 (1976).

(17) J. Stöhr, G. Apai, P.S. Wehner, F.R. McFeely, R.S. Williams, and D.A. Shirley, Phys. Rev. B14, 5144 (1976).

(18) L.F. Wagner, Z. Hussain, and C.S. Fadley, Solid State Commun. 21, 257 (1977).

(19) J. Stöhr, P.S. Whener, R.S. Williams, G. Apai, and D.A. Shirley, Phys. Rev. B17, 587 (1978).

(20) D.A. Shirley, R.S. Williams, P.S. Wehner, R.F. Davis, and S.D. Kevan, Lawrence Berkeley Laboratory Report LBL-9344 (July 1979).

(21) R.S. Williams, P.S. Wehner, J. Stöhr, and D.A. Shirley, Phys. Rev. Letters 39, 302 (1977).

(22) T. Grandke, L. Ley, and M. Cardona, Phys. Rev. Letters 38, 1033 (1977).

(23) T. Grandke, L. Ley, and M. Cardona, Phys. Rev. B18, 3847 (1978).

(24) P. Thiry, R. Pinchaux, G. Martinez, Y. Petroff, J. Lecante, J. Paigne, Y. Ballu, C. Guillot, and D. Spanjaard, Solid State Commun. 27, 99 (1978).

(25) K. Mills, D. Denley, P. Perfetti, and D.A. Shirley, Solid State Commun. 30, 743 (1979).

(26) T. Chiang, J.A. Knapp, D.E. Eastman, and M. Aono, IBM Research Report RC 7605 (#32921) April 1979. (Unpublished)

(27) P. Citrin, G.K. Wertheim, and Y. Baer, Phys. Rev. Letters 41, 1425 (1978).

(28) Tran Minh Duc, C. Guillot, Y. Lassailly, J. Lecante, Y. Jugnet, and J.C. Vedrine, Phys. Rev. Letters 43, xxx(1979).

(29) Y. Petroff, private communication, August 1979.

(30) W.T. Bordass and J.W. Linnett, Nature 222, 660 (1969).

(31) T. Gustafsson, W. Plummer, and D.E. Eastman, Solid State Commun. 17, 391 (1975).

(32) J.W. Cooper, Phys. Rev. Letters 13, 762 (1964).

(33) U. Fano and J.W. Cooper, Rev. Med. Physico 40, 441 (1968).

(34) G. Apai, P.J. Wehner, J. Stöhr, R.S. Williams, and D.A. Shirley, Solid State Commun. 20, 1141 (1976).

(35) J.N. Miller, D.T. Ling, I. Lindau, P.M. Stefan, and W.E. Spicer, Phys. Rev. Letters 38, 1419 (1977).

(36) P.S. Wehner, S.D. Kevan, R.S. Williams, R.F. Davis, and D.A. Shirley, Chem. Phys. Letters 57, 334 (1978).

(37) R.F. Davis, S.D. Kevan, B.-C. Lu, J.G. Tobin, and D.A. Shirley, "Condensed Phase Photoelectron Asymmetry," Lawrence Berkeley Laboratory Report LBL-9384 (July 1979); submitted to Phys. Rev. Letters.

(38) C.N. Yang, Phys. Rev. 74, 764 (1948).

(39) D.J. Kennedy and S.T. Manson, Phys. Rev. A5, 227 (1971).

(40) A. Liebsch, Phys. Rev. Letters 32, 1203 (1974); Phys. Rev. B15, 544 (1976).

(41) D.P. Woodruff, D. Norman, B.W. Holland, N.V. Smith, H.H. Farrell, and M.M. Traum, Phys. Rev. Letters 41, 1130 (1978).

(42) N. Smith, private communication, March 1979.

(43) S. Kono, C.S. Fadley, N.F.T. Hall, and Z. Hussain, Phys. Rev. Letters 41, 117 (1978).

(44) S. Kono, S.M. Goldberg, N.F.T. Hall, and C.S Fadley, Phys. Rev. Letters 41, 1831 (1978).

(45) S.Y. Tong and M.A. Van Hove, Solid State Commun. 19, 543 (1976).

(46) S.Y. Tong and N. Stoner, J. Phys. C11, 3511 (1978).

(47) C.H. Li and S.Y. Tong, Phys. Rev. B19, 1769 (1979).

(48) C.H. Li and S.Y. Tong, Phys. Rev. Letters 42, 901 (1979).

(49) S.Y. Tong, private communication, March 1979.

(50) S.D. Kevan, D.H. Rosenblatt, D.R. Denley, B.-C. Lu, and D.A. Shirley, Lawrence Berkeley Laboratory Report LBL-9024, April 1979. (Phys. Rev. B, to be published)

(51) S.D. Kevan, D.H. Rosenblatt, D.R. Denley, B.-C. Lu, and D.A. Shirley, Phys. Rev. Letters 41, 1565 (1978).

(52) S.D. Kevan, unpublished data (August 1979).

(53) G.P. Williams, F. Cerrina, I.T. McGovern, and G.J. Lapeyre, to be published.

Figure Captions

Figure 1. Photon flux at the 4° branch of Beam Line I at SSRL, as measured by the photocurrent on a calibrated NBS photodiode, for "old" optical elements. With new elements the intensity recovers substantially above 280 eV, but within a few weeks it reverts to this form. From Ref. 7.

Figure 2. Comparison of the (inverted) transmission spectrum on the 4° branch line at SSRL (solid curve) with the absorption curve for polycrystalline graphite (dashed curve). Saturation effects and crystallite orientation differences preclude exact comparisons of intensities, but the coincidence of energies of features gives strong evidence that optical-element overlayers are graphitic rather than carbidic or polymeric.

Figure 3. Valence-band dispersion relations for Cu along $\Gamma\Lambda L$ as derived from angle-resolved photoemission spectra in the range $h\nu$ = 7-200 eV, as shown across the top. In the DTM analysis the initial and final k values are the same, modulo a G vector. Thus the valence bands can be unambiguously plotted by repeating in an extended-zone scheme, as shown. After Ref. 20.

Figure 4. Temperature dependence of the normal photoemission spectrum from a Cu(110) crystal at $h\nu = 45$ eV. At the highest temperature, density-of-states behavior is apparent.

Figure 5. Relative d-band intensities of five metals as functions of photon energy. Note the Cooper minima in Pd and Ag.

Figure 6. Photoemission spectra of the CO/Pd system at several photon energies. Note enhancement of the CO-derived features at $\sim$8 eV and 11 eV, for photon energies near 130 eV.

Figure 7. A comparison of $\sigma(\varepsilon)$ and $\beta(\varepsilon)$ results for the 4s and 4d shells of silver (Z = 47) with calculated values for atomic xenon (Z = 54), from Ref. 39. The experimental σ scale is only relative. The 4s shell shows $\beta \sim 2$, while for the 4d case both the Cooper minimum in $\sigma(\varepsilon)$ and the modulation in $\beta(\varepsilon)$ are qualitatively reproduced.

Figure 8. A series of normal photoelectron spectra for p(2×2)Se/Ni(001), at several photon energies. The Ni valence band is shown near zero binding energy. The next peak is Se(3d), then Ni(3p). Note the modulations of peak intensities with photon energy.

Figure 9. Normal photoemission intensity versus electron kinetic energy for Ni(3p), Se(3d), and Ni(valence band) peaks from p(2×2)Se/Ni(001). Note that the diffraction maxima fall at different energies. From Ref. 50.

Figure 10. Comparison of NPD for Se(3d) in disordered overlayers on Ni(001) and in the c(2×2) structure. From Ref. 50.

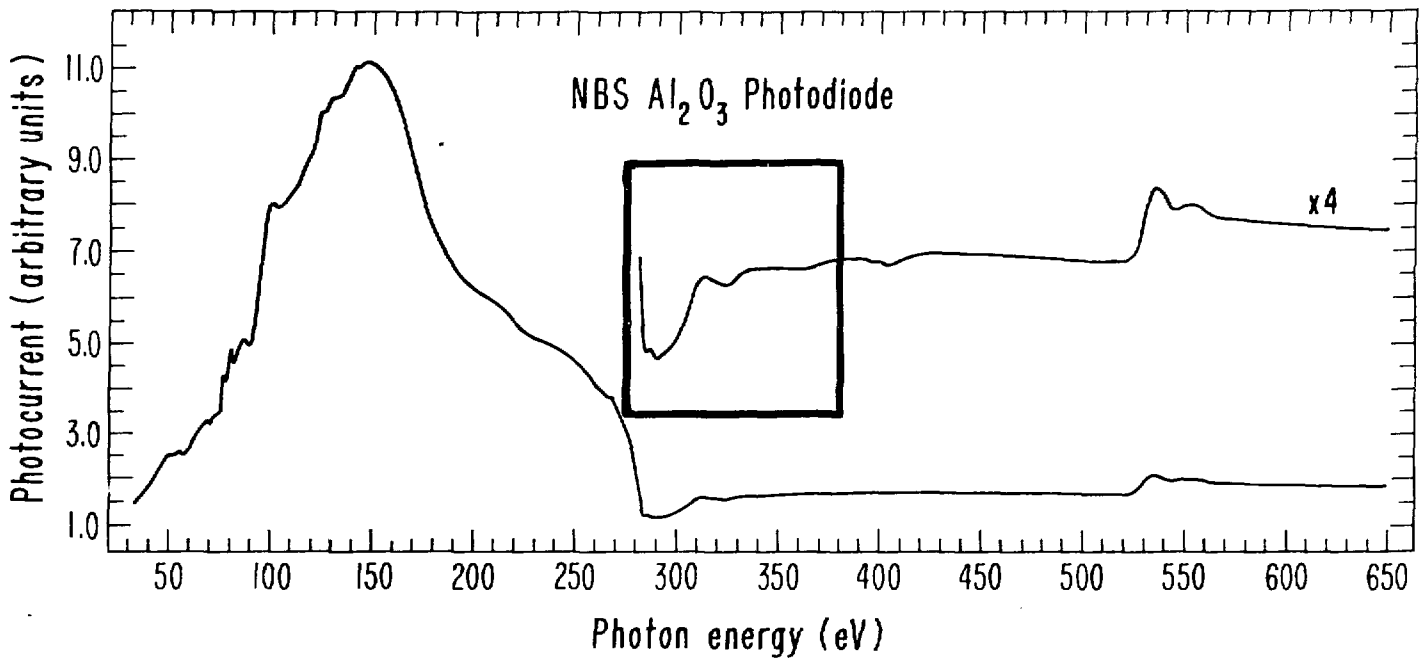

XBL 783-7465

Figure 1

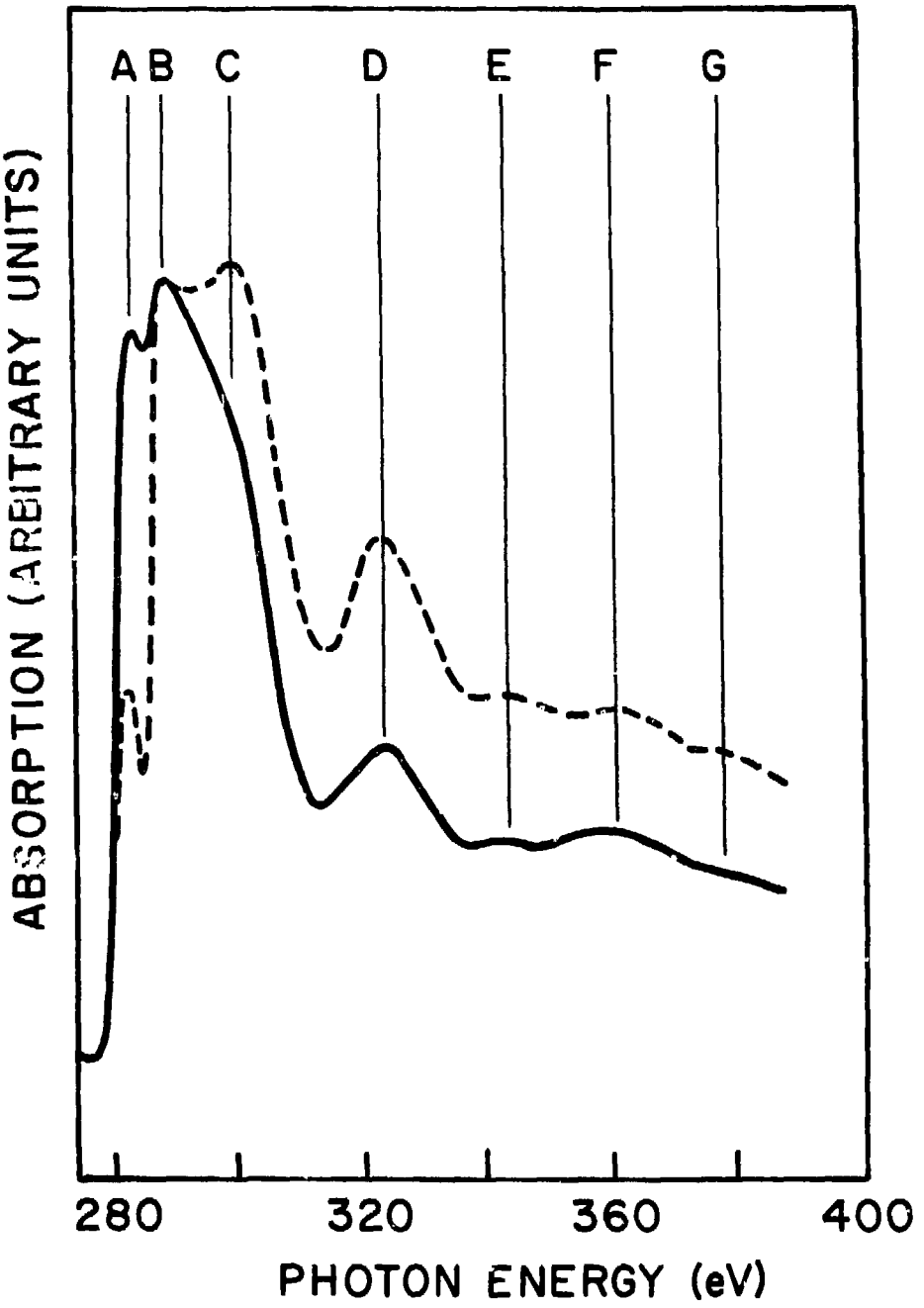

XBL 798-10803

Figure 2

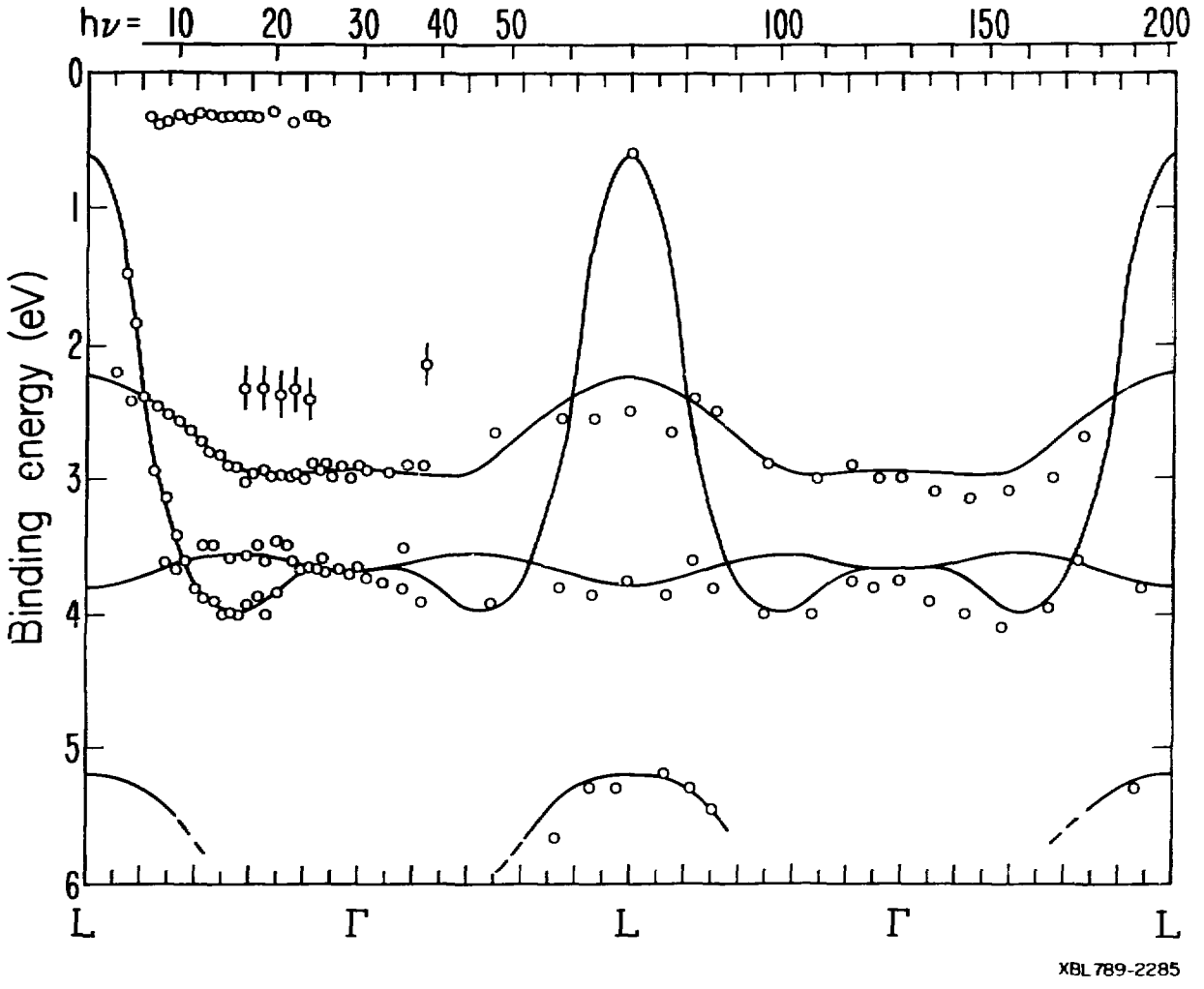
hν = 10 20 30 40 50 100 150 200
0
1
2
3
4
5
6
Binding energy (eV)
L
Γ
L
Γ
L
XBL 789-2285

Figure 3

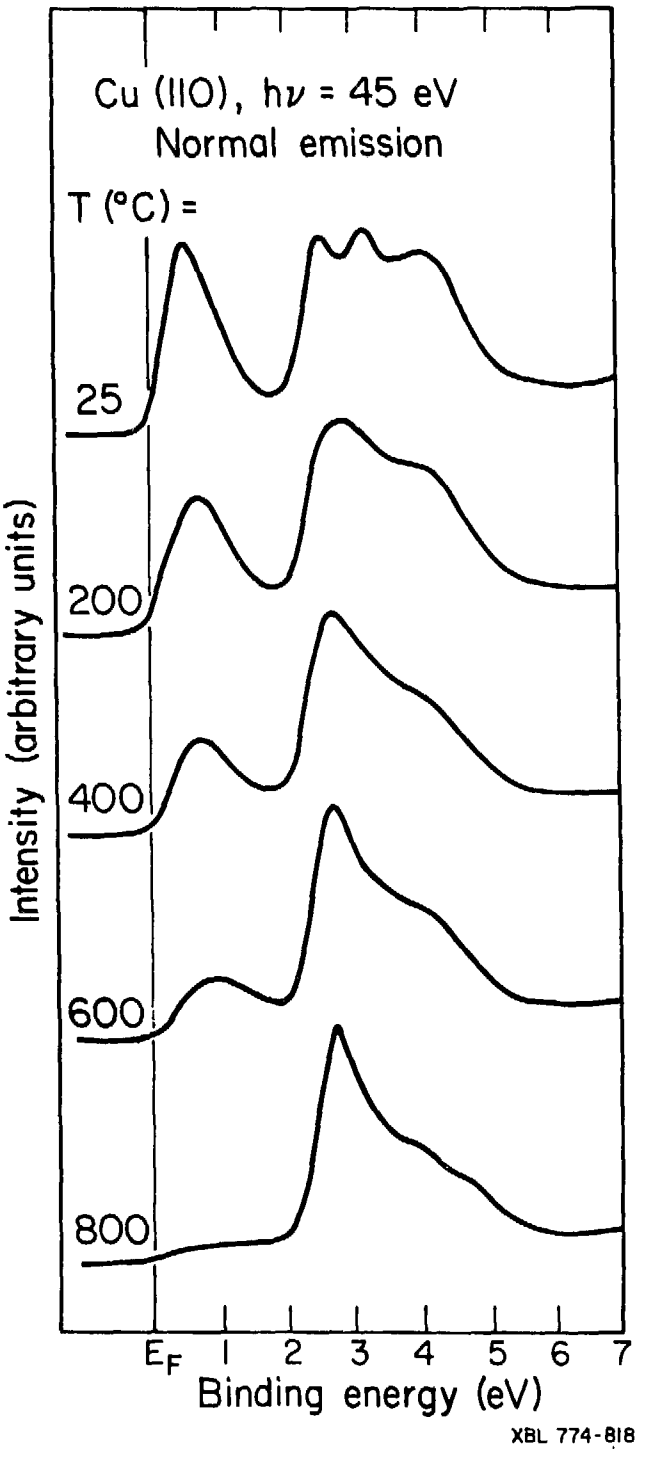
Cu (110), hν = 45 eV
Normal emission
T (°C) =
25
200
400
600
800
Intensity (arbitrary units)
E_F
1
2
3
4
5
6
7
Binding energy (eV)
XBL 774-818

Figure 4

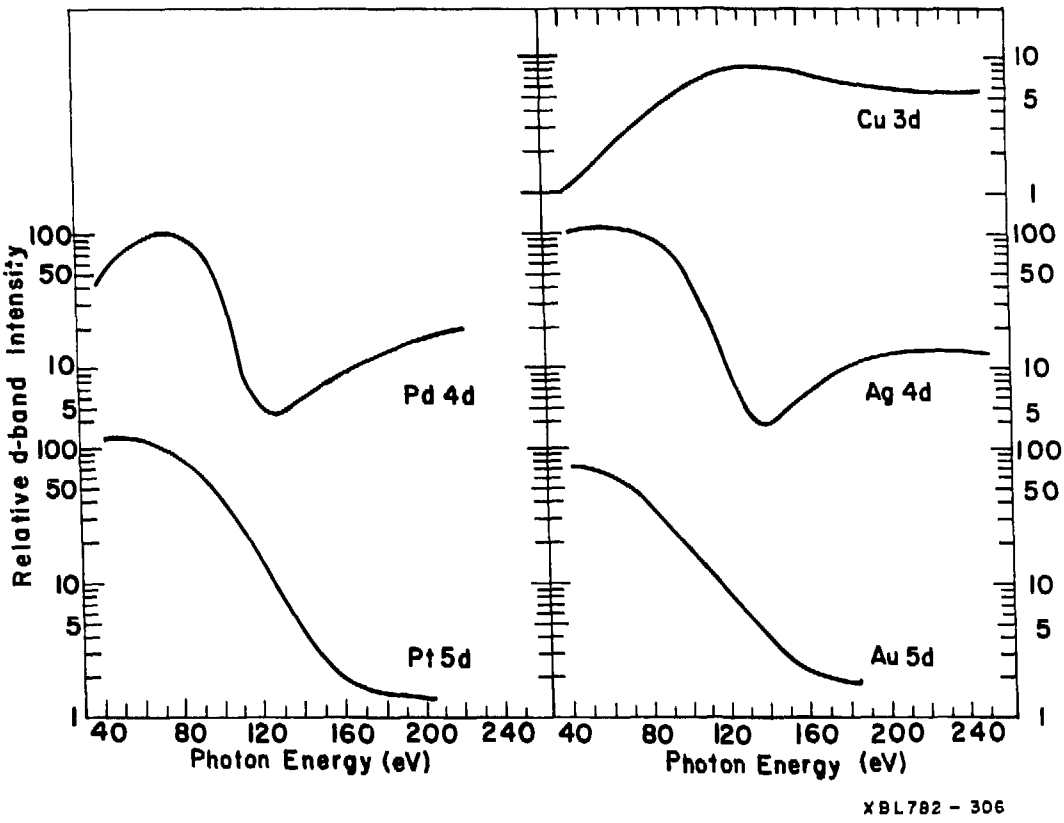
Relative d-band Intensity
Pd 4d
Pt 5d
Cu 3d
Ag 4d
Au 5d
Photon Energy (eV)
Photon Energy (eV)
XBL782 - 306

Figure 5

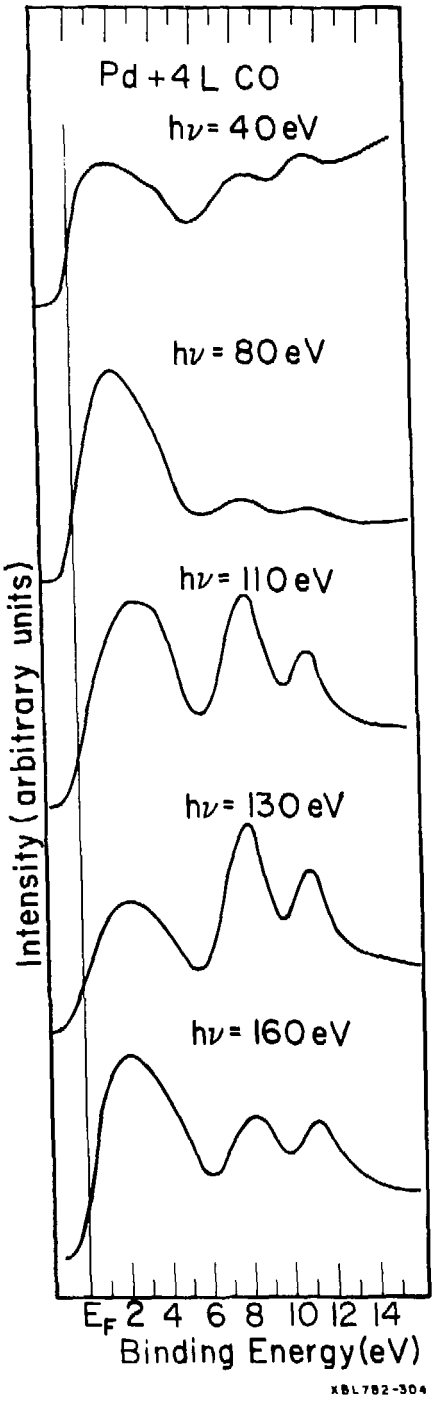
Pd + 4 L CO
hν = 40 eV
hν = 80 eV
hν = 110 eV
hν = 130 eV
hν = 160 eV
Intensity (arbitrary units)
E_F 2 4 6 8 10 12 14
Binding Energy (eV)
XBL782-304

Figure 6

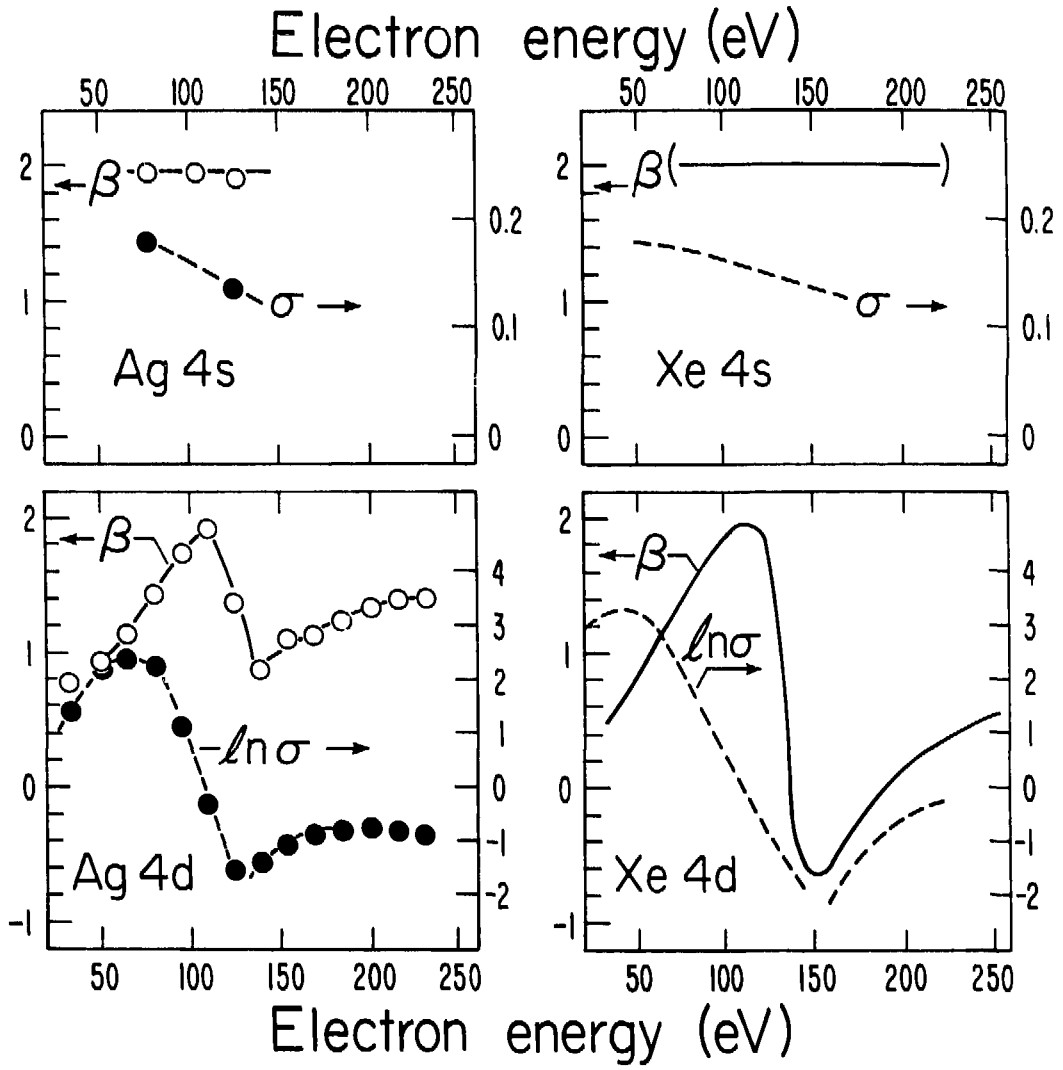

XBL 797-2104

Figure 7

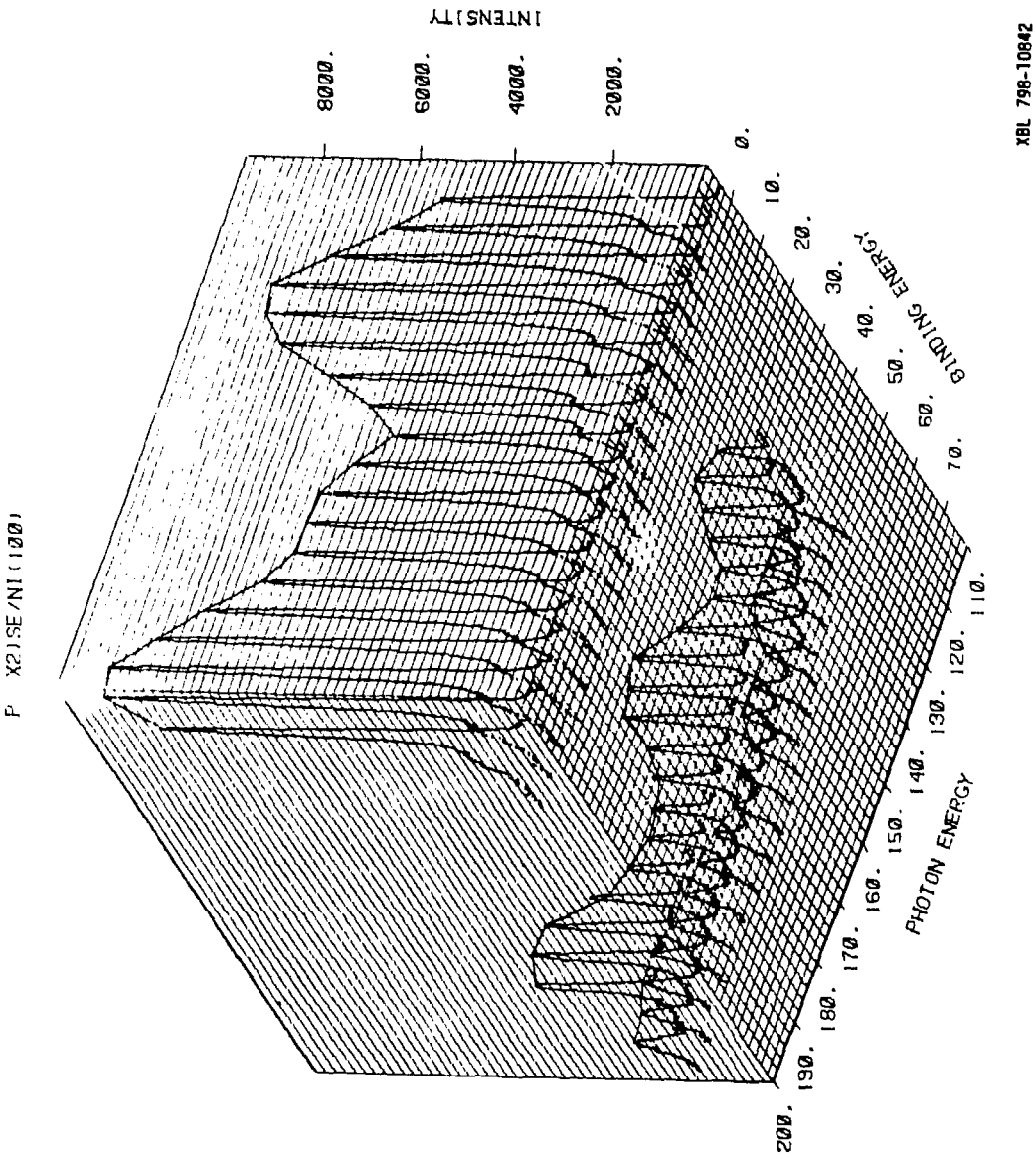
P X2)SE/NI(100)
INTENSITY
8000.
6000.
4000.
2000.
0.
10.
20.
30.
40.
50.
60.
70.
BINDING ENERGY
110.
120.
130.
140.
150.
160.
170.
180.
190.
200.
PHOTON ENERGY
XBL 798-10842

Figure 8

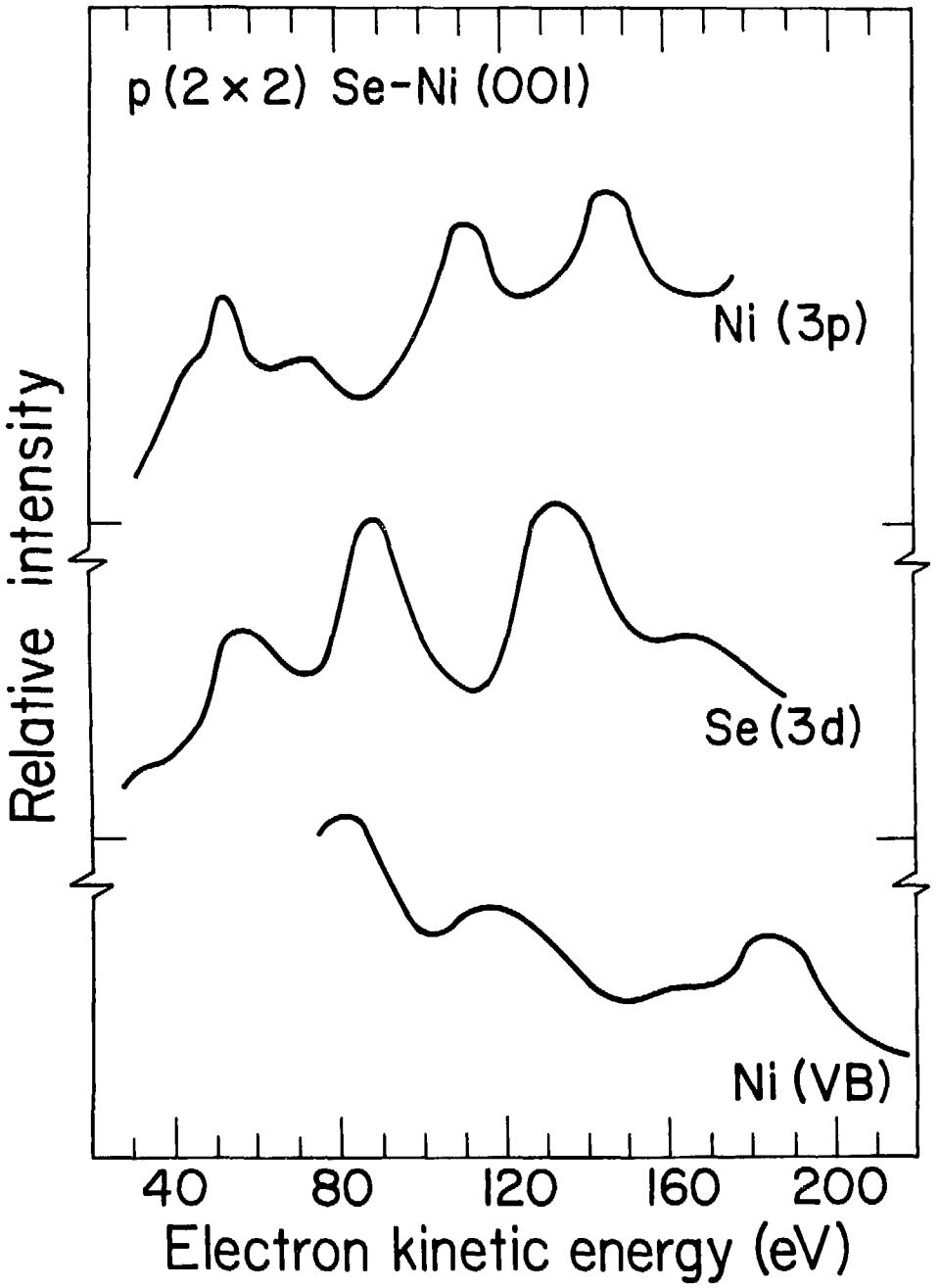
p(2×2) Se-Ni (001)
Ni (3p)
Se (3d)
Ni (VB)
Relative intensity
40
80
120
160
200
Electron kinetic energy (eV)
XBL 794-1374

Figure 9

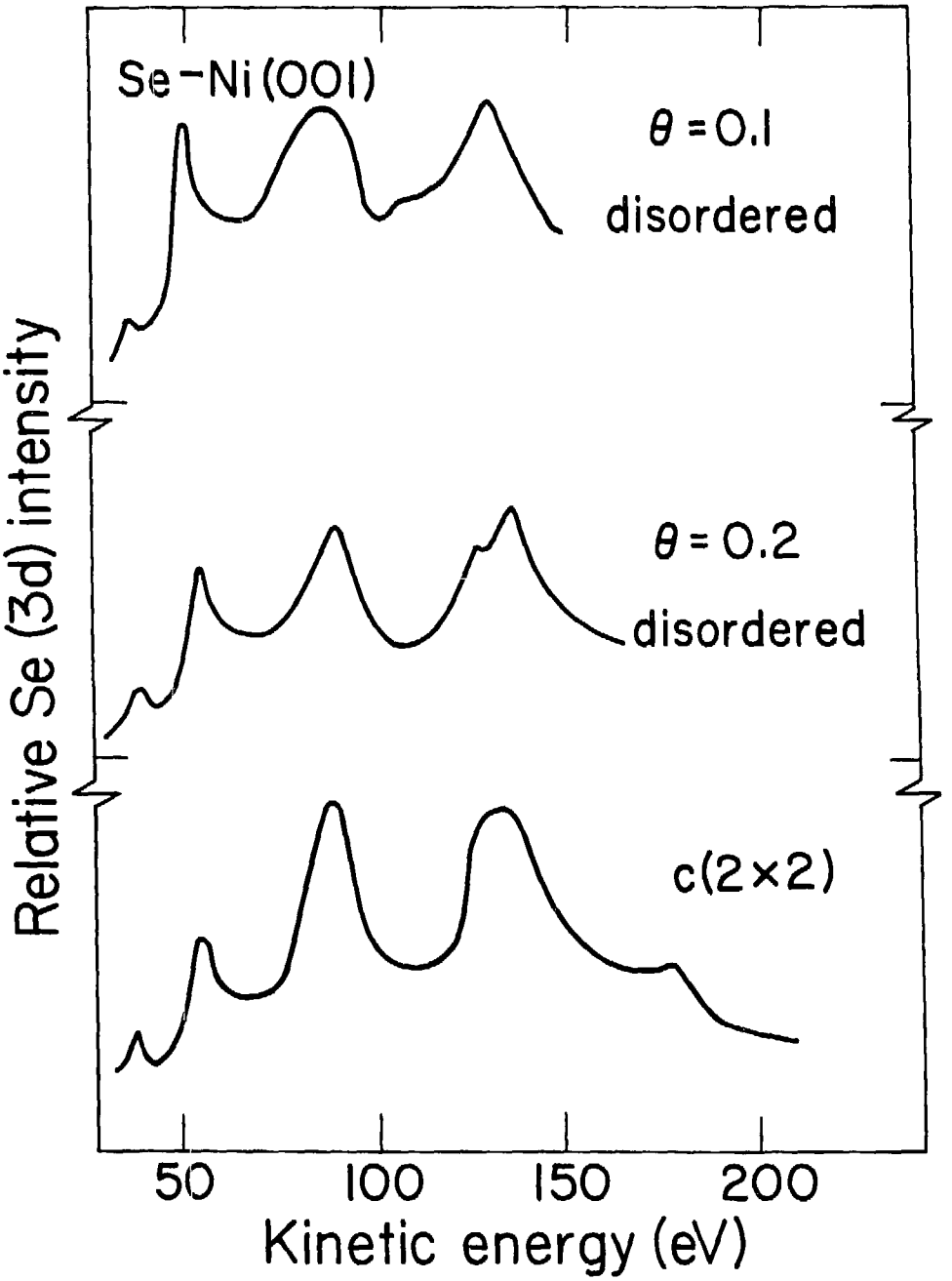

XBL 794-1376

Figure 10